Evidence of a topographic signal in surface soil moisture derived from ENVISAT ASAR wide swath data

Evidence of a topographic signal in surface soil moisture derived from ENVISAT ASAR Wide Swath data.

D.C. Mason[1], J. Garcia-Pintado[2], H.L. Cloke[12], S.L. Dance[23].

[1]Department of Geography and Environmental Science, University of Reading, Reading RG6 6AB, UK (d.c.mason@reading.ac.uk, h.l.cloke@reading.ac.uk).

[2]Department of Meteorology, University of Reading, Reading RG6 6AL, UK (j.garcia-pintado@reading.ac.uk, s.l.dance@reading.ac.uk).

[3]Department of Mathematics and Statistics, University of Reading, Reading RG6 6AX, UK.

Abstract

The susceptibility of a catchment to flooding is affected by its soil moisture prior to an extreme rainfall event. While soil moisture is routinely observed by satellite instruments, results from previous work on the assimilation of remotely sensed soil moisture into hydrologic models have been mixed. This may have been due in part to the low spatial resolution of the observations used. In this study, the remote sensing aspects of a project attempting to improve flow predictions from a distributed hydrologic model by assimilating soil moisture measurements are described. Advanced Synthetic Aperture Radar (ASAR) Wide Swath data were used to measure soil moisture as, unlike low resolution microwave data, they have sufficient resolution to allow soil moisture variations due to local topography to be detected, which may help to take into account the spatial heterogeneity of hydrological processes. Surface soil moisture content (SSMC) was measured over the catchments of the Severn and Avon rivers in the South West UK. To reduce the influence of vegetation, measurements were made only over homogeneous pixels of improved grassland determined from a land cover map. Radar backscatter was corrected for terrain variations and normalised to a common incidence angle. SSMC was calculated using change detection.

To search for evidence of a topographic signal, the mean SSMC from improved grassland pixels on low slopes near rivers was compared to that on higher slopes. When the mean SSMC on low slopes was 30-90%, the higher slopes were slightly drier than the low slopes. The effect was reversed for lower SSMC values. It was also more pronounced during a drying event. These findings contribute to the scant information in the literature on the use of high resolution SAR soil moisture measurement to improve hydrologic models.

Corresponding author: D.C. Mason (email: d.c.mason@reading.ac.uk, tel: +44-118-378-8740, fax : +44-118-975-5865).

Keywords: Soil moisture, Synthetic aperture radar, Hydrologic model

1. Introduction

One factor that affects the susceptibility of a catchment to flooding is its soil moisture condition prior to an extreme rainfall event. The antecedent soil moisture affects runoff because it controls the ability of the watershed to partition rainfall between infiltration and runoff. The improved representation of antecedent soil moisture in hydrologic models should therefore improve runoff prediction. Field studies show that the distribution of a catchment's water is controlled by soil water storage, with runoff rising abruptly when a certain storage threshold is exceeded (Lacava et al. 2012). It has been argued that soil water stored in hillslope areas is released only during wetter conditions, when flow paths between the hillslope and riparian zone become connected. Therefore, monitoring the closeness to thresholds is essential to accurately predict stream responses to rainfall events. One approach to this is through the measurement of soil moisture.

This paper describes the first stage of a study attempting to improve a distributed hydrological model for a set of catchments by assimilating remotely sensed soil moisture in order to keep the model flow rate predictions on track in readiness for an intense rainfall event, and to estimate model parameters. As remotely sensed soil moisture data from passive and active radars are obtained as area averages rather than point measurements, they form a useful source of synoptic data for assimilation in un-gauged catchments, the class to which the majority belong (e.g. Vorosmarty et al. 1996).

Despite the fact that soil moisture and runoff should be correlated, it is currently an open question how much assimilation of remotely sensed soil moisture into a hydrologic model can aid runoff prediction in un-gauged basins (Parajka et al. 2005). There seem to be a number of reasons for this (Crow and Ryu 2009). Firstly, for very intense rainfall events, antecedent soil moisture conditions may be of minor importance as the infiltration excess overland flow mechanism is dominant and rainfall runs off before it has the opportunity to infiltrate. Secondly, for basins lacking rain gauges, the main uncertainty will be due to the error in forecast rainfall rather than that due to soil moisture. Thirdly, the relationship between antecedent soil moisture and runoff is strongly non-linear and characterised by sharp thresholds that are unsuited to the application of data assimilation techniques designed for linear models (e.g. Kalman-derived filters and variational techniques).

A fourth reason that we investigate here is the low spatial resolution of the microwave soil moisture data (e.g. from ASCAT (Advanced Scatterometer), AMSR-E (Advanced Microwave Scanning Radiometer) or SMOS (Soil Moisture and Ocean Salinity satellite)) used in many previous studies (e.g. Parrens et al. 2012, Brocca et al. 2012a, 2012b, Lacava et al. 2012) compared to the 1km resolution of a typical hydrologic model. While a SMOS pixel (40x40km) is a lot larger than a typical un-gauged small catchment (say 10x10km), a 1km resolution would allow soil moisture variations within a small catchment to be detected, and would take into account the spatial heterogeneity of hydrological processes. For example, soil moisture contribution to runoff probably depends on distance to channel and local slope.

Vinnikov et al. (1996) have investigated the spatial and temporal length scales of soil moisture variability in deeper layers. They separated the variability of the soil moisture field into small- and large-scale components. The small-scale component is due to varying topography, soil type and land cover at the local scale. The large-scale component is due to wide-area atmospheric forcing. In the spatial domain, for the 0-10cm soil layer, they found that 30-35% of the total variance was due to small-scale land surface-related variability, and that this had a length scale of tens of metres. On the other hand, the atmospheric-related component had a length scale of 400-800km. This means that low resolution microwave sensors measure only the large-scale atmospheric-related component of soil moisture variations because they average out the small-scale topographic variations. Wagner et al. (1999) showed that the low correlations found between area-extensive ERS (European Remote Sensing satellite) scatterometer measurements and point field soil moisture measurements must be caused by the small-scale variability of the soil moisture field. High resolution remotely sensed soil moisture measurement should be capable of going at least some of the way towards observing this local variability.

Soil moisture can be measured at higher resolution using active SARs rather than passive sensors. Recently there has been increasing interest in estimating soil moisture at local scales using these sensors (Barrett et al., 2009). Two new active SARs suitable for catchment hydrology studies should begin producing data this year. The first of the Sentinel-1 satellites was launched in early 2014. Sentinel-1 is C-band, which will penetrate 1 - 2 cm into the soil. Hornacek et al. (2012) have proposed a near real-time automatic system for measuring surface soil moisture at 1km resolution using the Interferometric Wide Swath mode of Sentinel-1. This will measure soil moisture to 6% accuracy, and should be high enough resolution for catchment-scale hydrology studies. When the second satellite of the pair is launched 18 months after the first, they should give near daily coverage over Europe. Also, the Soil Moisture Active Passive sensor (SMAP) is due to be launched early this year (Entekhabi et al., 2010). SMAP is L-band, which will penetrate ~5 cm into the soil (Kerr et al., 2001). It is a combined low resolution radiometer and high resolution SAR, which should give 4% soil moisture accuracy in its 9km resolution product. There is also a radar-only 3km product which will be less accurate. However, possibly this will not be high enough spatial resolution for catchment-scale hydrology studies.

However, from the point of view of this study, obviously these cannot yet provide images of any sequence of flood events that could be analysed. For the Distributed Hydrologic Model Inter-comparison project phase 2 (Smith et al 2012), 11 years of data were needed, with a model warm-up period of 1 year, a calibration period of 6 years, and a verification period of 4 years. As a result, we have used ASAR data for this study. ASAR Wide Swath (WS) data were acquired from 2003 – 2011, giving a long data record. ASAR is C-band, which penetrates soil to 1 – 2 cm. ASAR WS has a spatial resolution of approximately 150m (75m pixel size) and a 400km swath width. VV polarisation images were chosen because of their higher capability of vegetation penetration compared to HH polarisation (Kong and Dorling, 2008). A difficulty with ASAR WS is that the time interval between successive scene acquisitions can be irregular in many areas. For example, in the data set used in this study, there were on average two scenes per month, but in several months there were no useable scenes at all.

There appears to be scant information in the literature relating to the use of high resolution SAR soil moisture measurement to improve rainfall-runoff estimation. Previous soil moisture studies using high resolution SAR have been aimed mainly at estimating surface soil moisture content (SSMC). Considering ASAR WS data, Loew et al. (2006) have derived soil moisture from the backscattering cross-section for various agricultural land covers (including grassland), and concluded that soil moisture can be measured to 5.7 vol% over a range 15 – 40 vol%. Kong and Dorling (2008) used a principal component analysis to show that surface roughness, vegetation and topographic effects could be partially separated (see also Verhoest et al., 1998). ASAR WS data have also been used to study soil moisture variations at high resolution in an alpine valley (Greifeneder et al. 2014); to validate soil moisture measurements from passive microwave sensors at a number of Irish sites (Pratola et al., 2014); and to map surface soil moisture over parts of Tunisia (Zribi et al., 2014). Other high resolution SARs have also been applied to soil moisture measurement, for example multi-polarised RADARSAT-2 over wheat-growing areas (Yang et al., 2013). At somewhat lower resolution, ASAR global mode data have been used to estimate soil moisture at regional/continental scales in several studies (e.g. Pathe et al., 2009; Dostalova et al., 2014).

Early work to detect a topographic signal in soil moisture used airborne and ground measurements. Wang et al. (1989) used a push broom L-Band radiometer to map the spatial distribution of soil moisture. By using overlapping flight lines for several flights during a drying period, it proved possible to map the spatial patterns of soil moisture within a small watershed. This showed the top of the watershed drying out quicker than the floodplain. Roberts and Crane (1997), using ground measurements, also showed that an area on a sloping hillside dried out faster than the valley bottom below.

The object of this paper is to detect whether a topographic signal can be seen in high resolution remotely sensed soil moisture data. Such a signal may be useful information for a hydrologic model to be able to account for spatial heterogeneity in hydrological processes in relation to flood-producing rainfall-runoff events (e.g. Roberts and Crane 1997). The paper is an observational study, and contains no modelling. A subsequent paper will investigate whether the assimilation of these data into a hydrologic model is able to improve runoff prediction.

2. Study area and data set

The area considered in this study covered the catchments of the Severn and Avon rivers in the South West United Kingdom (fig. 1). This included the three main catchments of the Severn, Avon and Teme, and four other sub-catchments. The main catchments contain a number of

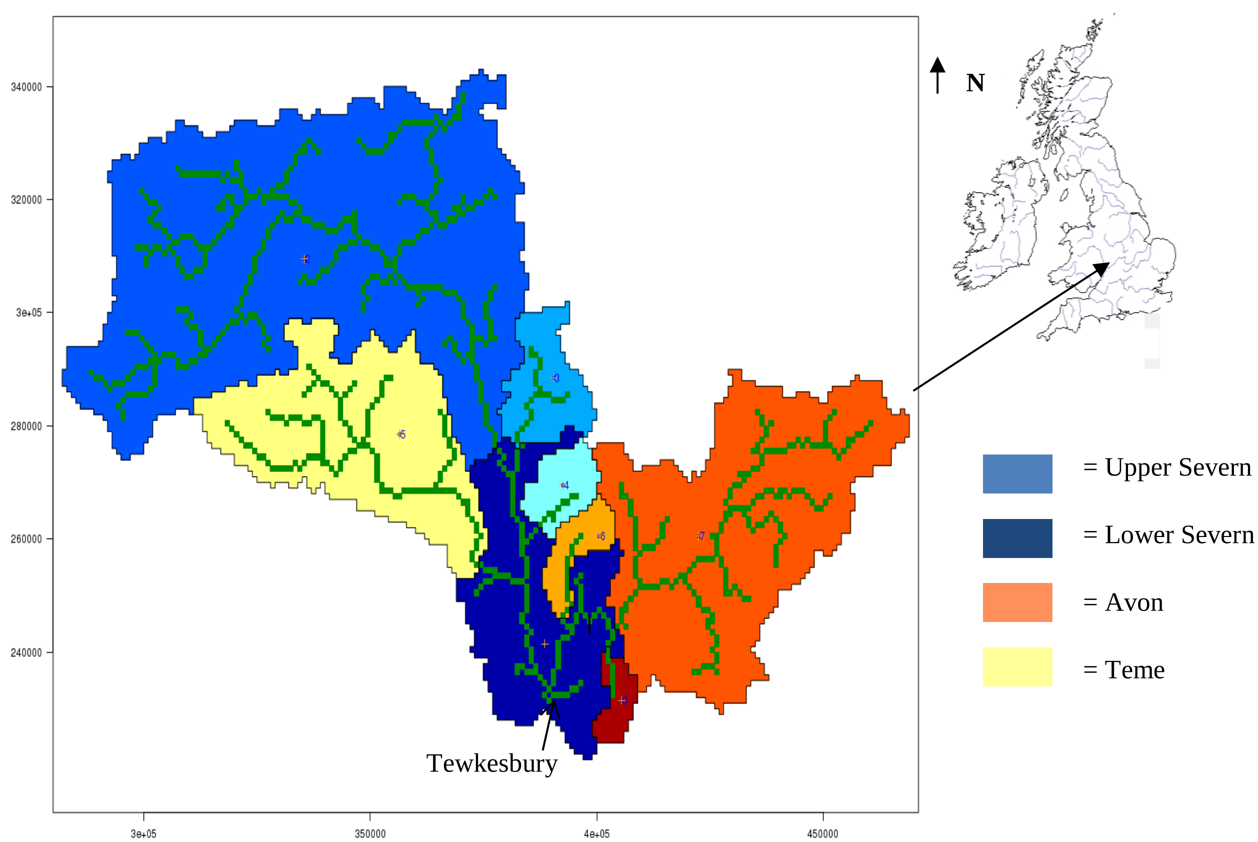

Figure 1. Severn/Avon catchments and sub-catchments.

gauges because the area floods on a reasonably frequent basis, though the sub-catchments are often un-gauged. The bounding rectangle of the area is 190km x 120 km. The southern boundary lies just below the town of Tewkesbury, which lies at the confluence of the Severn, flowing in from the north-west, and the Avon, flowing in from the north-east. The elevation range of the area is 10 – 300m AOD (Above Ordnance Datum), with most of the higher land in the west of the region. The mean slope is 7%, with a slope standard deviation of 8%. The predominant land cover types are improved grassland and arable. The surface soil layer is mainly fine textured clay. 42 ASAR WS scenes acquired between May 2006 and September 2008 were employed in the study. There was no significant snow cover on any of the images. Observed rainfall data during the period considered was obtained from a network of tipping bucket rainfall gauges sparsely distributed over the area.

3. Methods

3.1 ASAR WS processing chain

The ASAR WS processing chain is shown in fig. 2, and the most important steps are described below.

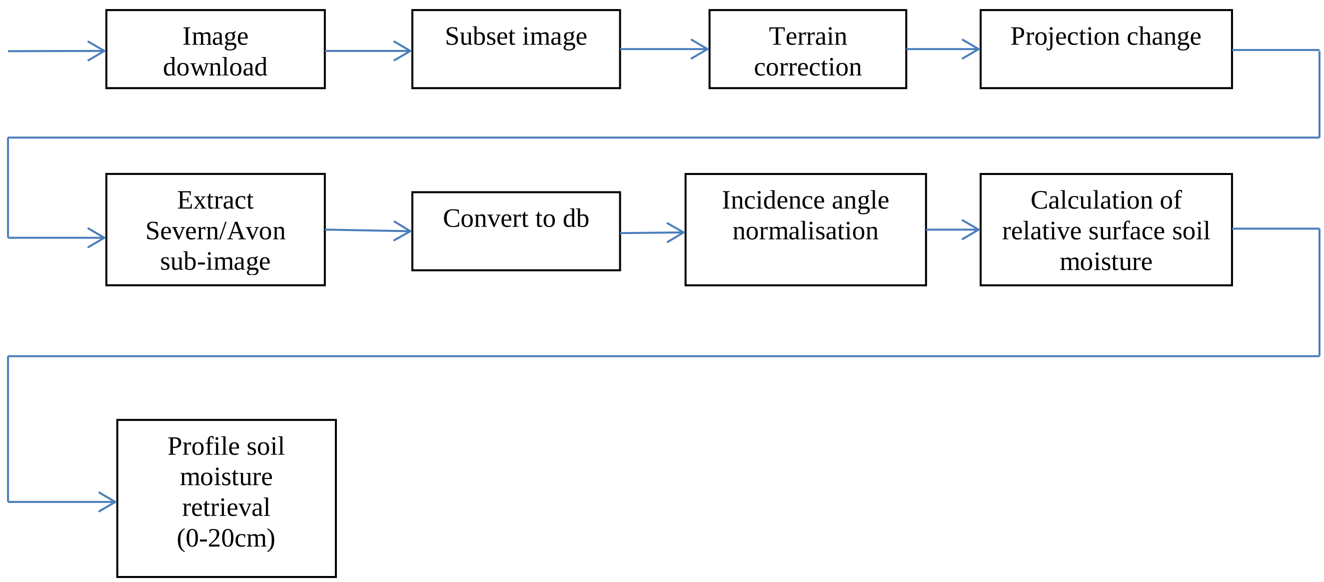

Figure 2. ASAR WS processing chain.

1) *Terrain correction*. A Range-Doppler Terrain Correction is applied to the geocoded sub-images of the Severn/Avon domain using the European Space Agency (ESA) NEST (Next ESA SAR toolbox) software and the Shuttle Radar Topography Mission (SRTM) Digital Elevation Model (DEM). Changes in local terrain slopes and aspect with respect to the incident wave will cause significant distortion in the radar backscatter intensities, and Loew et al. (2006) point out that it is mandatory to normalise the image data for terrain-induced backscatter changes. A radiometric normalisation is applied to each pixel's radar backscatter cross-section (σ^0) based on the local incidence angle to the DEM in the range plane and the local incidence angle to the ellipsoid in this plane at this pixel (Kellndorfer et al., 1998).

2) *Incidence angle normalisation*. A local incidence angle normalisation is applied for the improved grassland land cover class.

To cope with the fact that C-band data penetrates only 1-2 cm into the soil, soil moisture is only measured in large homogeneous regions having low local vegetation cover, namely areas of improved grassland. In the subsequent assimilation stage, soil moisture would only be assimilated into the hydrologic model in these regions, as it is neither necessary nor typical for a full grid of observations to be present for assimilation to proceed. Pixels of improved grassland in the Severn/Avon region (fig. 3) were selected using the CEH Land Cover Map, constructed from high resolution multispectral satellite data (Morton et al., 2011). The original map containing 25m pixels was averaged to produce 75m pixels to correspond to the ASAR WS pixel size. Because the ASAR WS spatial resolution is twice its pixel size, improved grassland pixels were only selected if a central 75m pixel and its border of 25m pixels were all classed as improved grassland. This avoided edge effects and ensured more homogeneous improved grassland pixels, so that problems caused by mixed pixels could be reduced. Pixels of other land cover types (arable, woodland, urban, water, etc) were ignored. Approximately one-third of the Severn/Avon region is classed as improved grassland, giving a substantial pixel sample size for measurements.

Radar backscatter generally shows a strong dependence on local incidence angle, with backscatter decreasing strongly with increasing incidence angle over sparsely vegetated terrain such as improved grassland (Pathe et al., 2009). Following Loew et al. (2006), a statistical approach was used to normalise the backscattering cross-section to a reference incidence angle of 23°, given an incidence angle range in the ASAR data of 15° - 45°. The SAR image data in homogeneous improved grassland pixels in the Severn/Avon domain were used to derive angular variations of the backscattering cross-section, based on 42 ASAR WS images from 2006-8. In

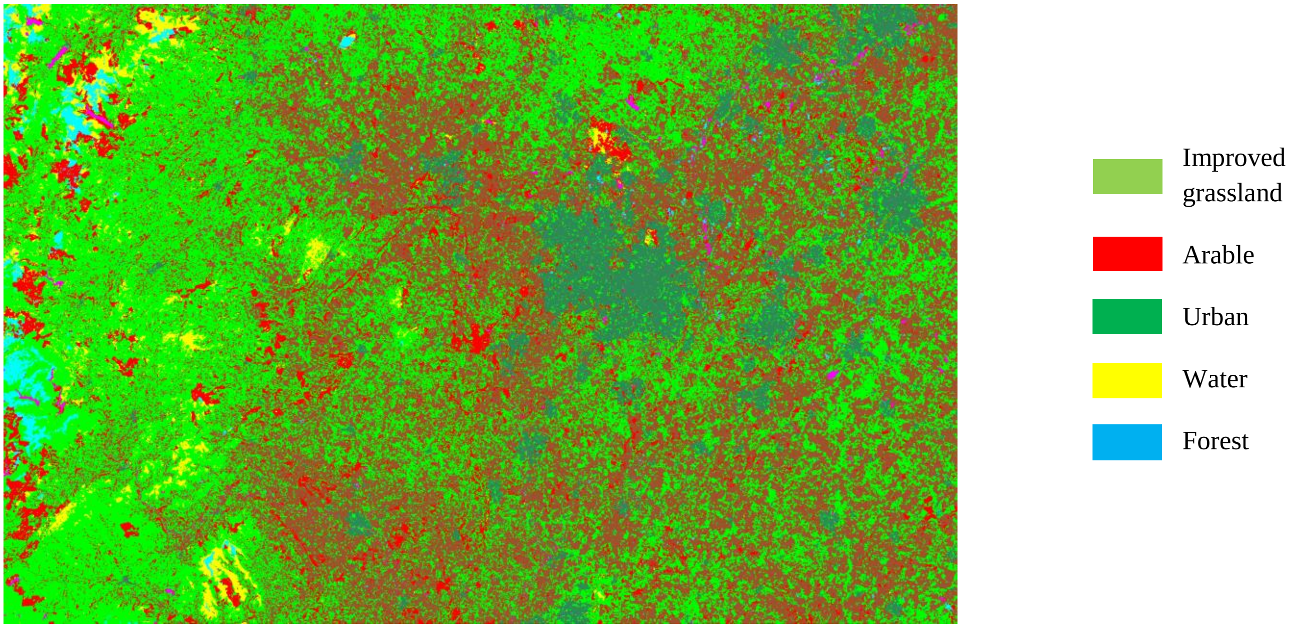

Figure 3. CEH Land Cover Map over Severn/Avon catchments.

common with other approaches, a simple linear model was fitted to data acquired over this period. The slope β of this was assumed to be constant over time. This ignores the effect of seasonal vegetation changes in the improved grassland class, which will cause the backscatter to change when the vegetation grows. However, as shown by Pathe et al. (2009), changes in backscatter due to vegetation growth are, in general, much smaller than changes due to soil moisture. A value for β of -0.093 ± 0.003 db/degree was found in the regression. Fig. 4 shows example normalised backscatter cross-section maps over the region for dry and wet periods.

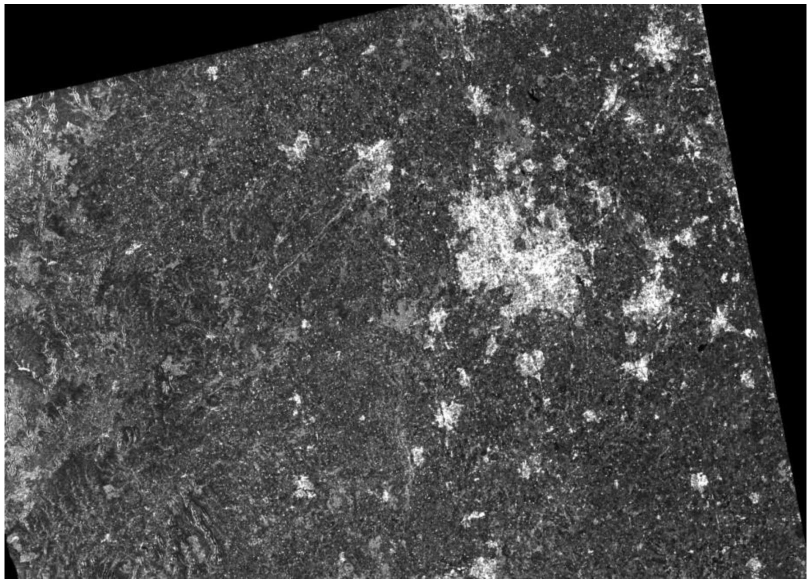

(a)

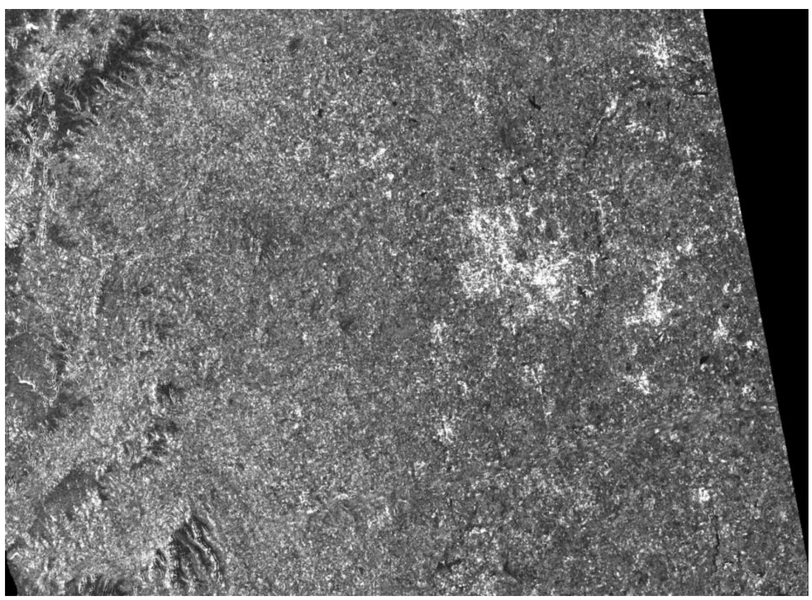

(b)

(b)

Figure 4. Normalised backscatter cross-section maps for (a) dry period (22/04/2007)), (b) wet period (07/01/2007) (over rural areas, brighter backscatter indicates wetter soil).

3) *Calculation of relative surface soil moisture content (SSMC).* The high temporal resolution of ASAR WS allows a dense image sequence to be acquired, which means that surficial soil moisture may be measured using a change detection technique (Wagner et al., 1999, Balenzano et al. 2011). Soil moisture measurement using change detection is based on the fact that variations in surface backscatter observed with a short repeat interval should mainly reflect changes in soil moisture, since changes of surface roughness, canopy structure and vegetation biomass will generally occur at longer temporal scales than soil moisture changes. The method estimates the degree of surface water soil saturation, from which the volume of water present in the soil relative to the volume of the soil's pores can be deduced (Hornacek et al. 2012). The change detection method has been shown to perform as well as a number of other methods for detecting SSMC (Gruber et al., 2014). Fig. 5 shows an example time series of the backscattering cross-section σ^0 for the improved grassland pixel at BNG (British National Grid) coordinates (339850E, 304100N) near the centre of the region for the period 01/05/2006 – 02/09/2008, for comparison with mean temperature and precipitation at this location.

The relative SSMC m_s is calculated using (Wagner et al., 1999) –

$$m_s = (\sigma^0 - \sigma^0_{dry}) / (\sigma^0_{wet} - \sigma^0_{dry}) \quad [1]$$

σ^0_{dry} and σ^0_{wet} are assumed to represent dry and wet soil conditions at a pixel respectively. Pathe et al. (2009) show that the absolute minimum and maximum values of σ^0 are in general poor estimators of σ^0_{dry} and σ^0_{wet} respectively. They adopt the approach of assuming that the numbers of scenes taken during dry (N_{dry}) and wet (N_{wet}) conditions are approximately known, then calculating the dry backscatter reference by averaging the N_{dry} lowest σ^0 values, and the wet reference by averaging the N_{wet} highest σ^0 values. If σ^0_{dry} and σ^0_{wet} are estimated from all the

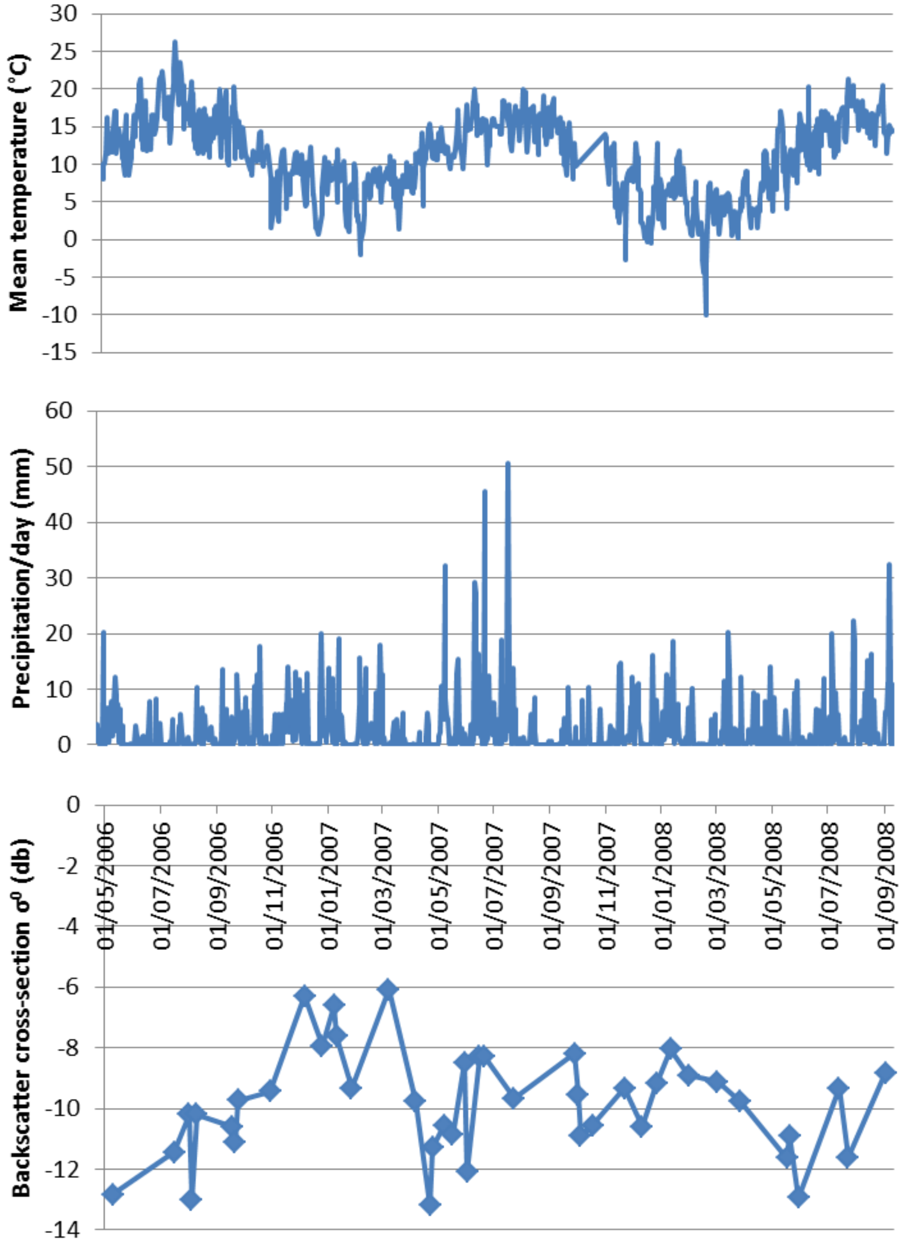

Figure 5. Time series of mean temperature, precipitation and backscatter cross-section σ^0 (db) for the improved grassland pixel at BNG coordinates (339850E, 304100N) for the period 01/05/2006 – 02/09/2008.

scenes, a difficulty is that wet scenes in which there is open flood water will have very low minimum values at the affected pixels, and these could be misinterpreted as being very dry. Many of these pixels can be removed from consideration by rejecting pixels having backscatters less than a low threshold (-14db), but some mixed pixels covering part land and part flood may remain. The solution that has been adopted is to calculate σ^0_{dry} at a pixel by taking the average of the three lowest values at the pixel from a set of dry images. The dry images are selected as those whose mean backscatter is in the lowest quartile of all the scenes. Similarly, σ^0_{wet} at a pixel is calculated by taking the average of the three highest values at the pixel from a set of wet images, which are selected as those whose mean backscatter is in the highest quartile of all the scenes. For example, for the improved grassland pixel in fig. 5, σ^0_{dry} = -13.0db, σ^0_{wet} = -6.3db, and the sensitivity range is 6.7db.

4) *Profile soil moisture retrieval*. The relative SSMC m_s is a measure of soil moisture only in the thin surface layer, whereas it is knowledge of the deeper root zone soil moisture (*RZSM*) that allows the assimilation to update the model soil moisture states at deeper layers. The approach taken here is to derive *RZSM* from m_s through the application of the exponential filter due to Wagner et al. (1999), so that *RZSM* rather than m_s may be assimilated (Brocca et al. 2012, Lacava et al. 2012).

The calculation of *RZSM* is a two-stage process. Firstly, a soil water index *SWI(t)* (0-1) is calculated for the 0-20cm profile at time *t* by forming a weighted average of the $m_s(t_i)$ values from the previous *i* ASAR measurements at time t_i ($t_i \leq t$). Each $m_s(t_i)$ value is weighted by the negative exponential $exp(-(t-t_i)/T)$ (see equation [6] of Wagner et al., 1999). *SWI(t)* is calculated if there is at least one ASAR measurement in the time interval [*t*-*T*, *t*] and at least three measurements in the interval [*t*-*5T*, *t*]. The parameter *T* was taken to be 15 days, as determined by Wagner et al. (1999). Secondly, *RZSM(t)* is calculated by combining *SWI*(*t)* with soil parameters (equation [7] of Wagner et al., 1999) -

$$RZSM(t) = W_{min} + SWI(t).(W_{max} - W_{min}) \qquad [2]$$

Here W_{min} was set to the wilting level and W_{max} to the field capacity for clay soil.

4. Results

4.1 Changes in remotely sensed relative surface soil moisture

In order to search for evidence of a topographic signal in the remotely sensed relative SSMC, we compared the mean relative SSMC from improved grassland pixels on low slopes (less than 7%) near rivers (greater than 0.1km and less than 0.8km from a river), with that from improved grassland pixels on higher slopes (7-20%) not necessarily near rivers. Constructing a mean relative SSMC for each class over the whole of the Severn/Avon catchment would not be sensible, as the rainfall history over such a large area would be unlikely to be uniform over the area, and there are more higher slopes in the west of the region than the east. Consequently the Severn/Avon catchment was divided up into 10km squares (i.e. each the size of a small catchment), with each square containing about 18000 75m ASAR WSM pixels. Within each square, the mean relative SSMC of improved grassland pixels in the low slope and higher slope classes was determined. Only 10km squares that contained 700 or more improved grassland pixels in each class were considered. There were about 50 such squares. Observed rainfall data from rain gauges was interpolated over the whole area to each 10km square using block kriging. Fig. 6 shows a plot of the difference between the mean relative SSMCs on low and higher slopes (low slope mean – higher slope mean) ($SSMC_D$) versus the mean relative SSMC on low slopes ($SSMC_L$), for all 10km squares for all 42 ASAR images. If there were no differences between the mean relative SSMCs on low and higher slopes at all $SSMC_L$ values, this would mean that no topographic signal was present between the two classes. However, a small difference is definitely apparent. From visual inspection, it appears that (a) at high $SSMC_L$ values, the $SSMC_D$ values are close to zero, as might be expected, (b) at medium $SSMC_L$ values, $SSMC_D$ values are slightly positive, and (c) at low $SSMC_L$ values, $SSMC_D$ values are slightly negative. This suggests that a second-order polynomial might be used to model the scatter plot. A second-order regression line is superimposed on fig. 6. The coefficients of the polynomial and their errors are given in table 1, together with the R^2 value (regression identifier R1). It can be seen that the first and second-order coefficients are significantly non-zero to a high degree. While the amount of variance accounted for by the regression is low ($R^2 = 0.086$), this is due to the substantial variation present in the samples. In a case where the R^2 value is low but the polynomial coefficients are statistically significant, it is still possible to draw valid conclusions about how changes in a coefficient value are associated with changes in the response value. Table 1 also gives the coefficients for a linear regression, which are also statistically significant, with the lower R^2 value showing the need for the polynomial regression (identifier R2).

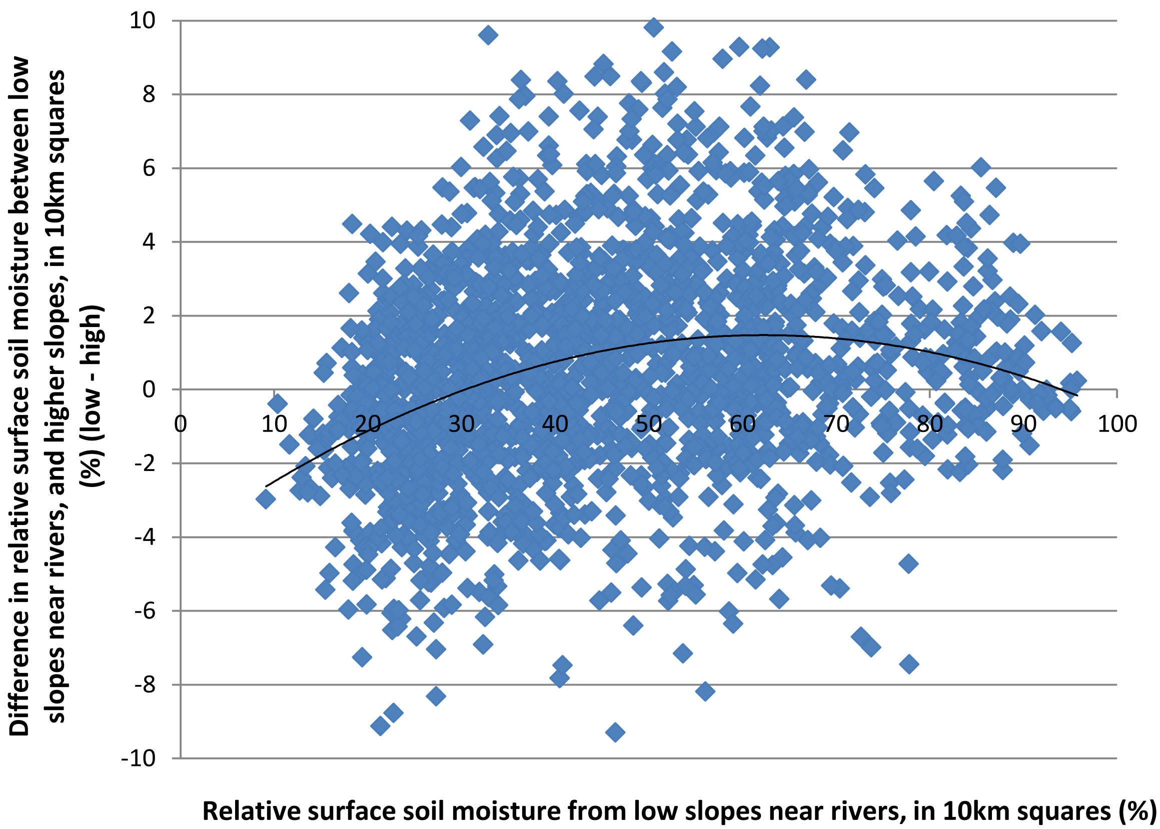

Figure 6. Mean relative SSMC difference between low slopes near rivers and higher slopes, versus mean relative SSMC of low slopes near rivers, in 10km squares, for all ASAR acquisitions. The black line is regression R1 of table 1.

Regression identifier	Type of regression	No. of samples	Relative SSM range %	Coefficient a	Coefficient b	Coefficient c	R^2
R1	Second-order polynomial	2011	10-90	-4.16 ± 0.39	0.181 ± 0.017	-0.00146 ± 0.00016	0.086
R2	Linear	2011	10-90	-1.10 ± 0.17	0.036 ± 0.003		0.051
R3	Second-order polynomial	259	10-70	-5.19 ± 1.57	0.192 ± 0.083	-0.00111 ± 0.00099	0.212

Table 1. Regressions of the difference between the mean relative SSMCs on low and higher slopes (low slope mean – higher slope mean) versus the mean relative SSMC on low slopes (a) for a second-order polynomial ($y = a + bx + cx^2$) for all 10km squares for all images, (b) for a linear regression ($y = a + bx$) for all 10km squares for all images, and (c) for a second-order polynomial for a rainfall scenario in which either <1mm of rain fell on the day of the acquisition and > 3mm fell on the previous day, or <1mm of rain fell on the acquisition day and the previous day and >3mm fell on the day before that.

From the plot it can be seen that (a) when $SSMC_L$ approaches 100%, there is little difference between the mean relative SSMC of the low and higher slopes, (b) when $SSMC_L$ is 30 - 90%, the higher slopes are slightly drier than the low slopes (from regression R1, a maximum of about 1.6% at an $SSMC_L$ of 60%), and (c) when $SSMC_L$ is low, the low slopes become slightly drier (about 2% maximum) than the higher slopes.

Fig. 6 has been produced for all 10 km squares with sufficient statistics for all ASAR acquisition dates. It contains samples that occurred during or immediately after rainfall, when it might be expected that the relative SSMC of low slopes near rivers might be the same as that of higher slopes. Fig. 7 shows a similar plot for 10km squares during a drying phase when it is known that rainfall occurred a day or two previously. The samples in the plot are ones for which either (a) <1mm of rain fell on the day of the acquisition and > 3mm fell on the previous day, or (b) <1mm of rain fell on the acquisition day and the previous day and >3mm fell on the day before that. A second-order polynomial has been fitted to the data, with coefficients given in table 1 (identifier R3). The first and second-order coefficients are again significantly non-zero, and the R^2 value of 0.212 explains more variance than the polynomial fit for Fig. 6. Fig. 7 shows that, when $SSMC_L$ is 35-70%, the higher slopes are drier than the low slopes to a greater extent than in Fig. 6, with the mean relative SSMC difference achieving a maximum of about 2.8% at an $SSMC_L$ of 70%.

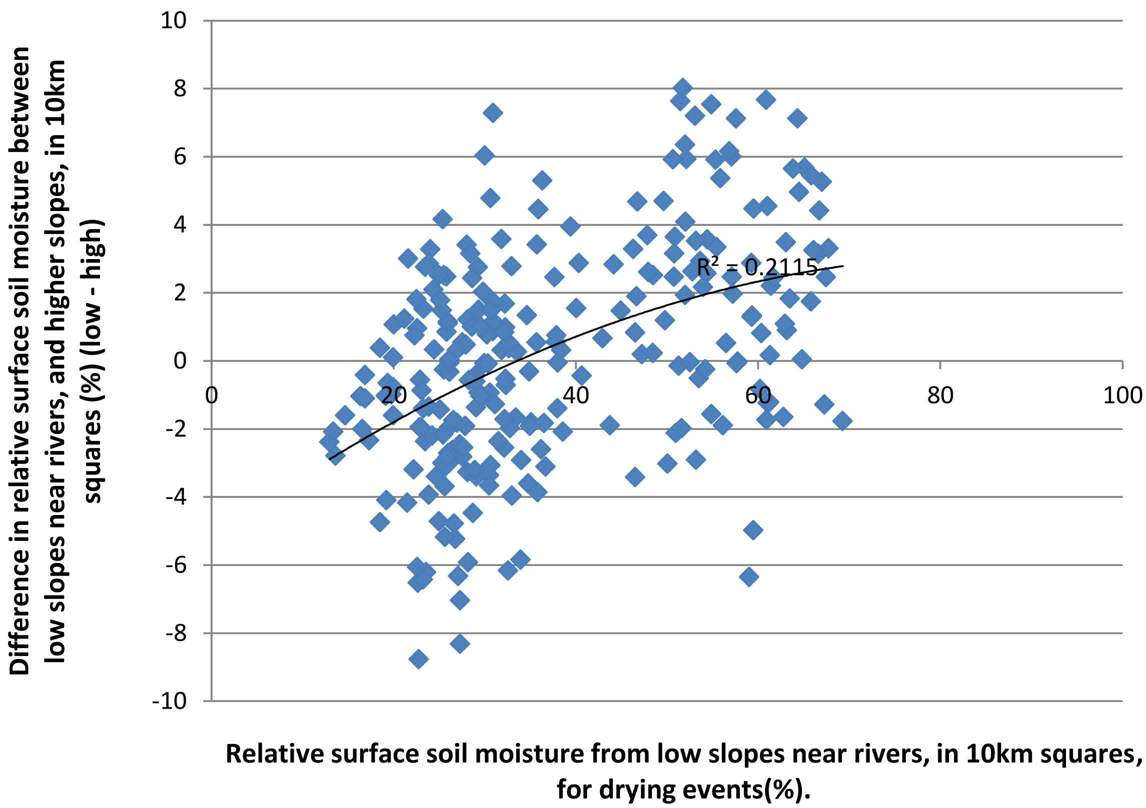

Figure 7. Mean relative SSMC difference between low slopes near rivers and higher slopes, versus mean relative SSMC of low slopes near rivers, in 10km squares, for a rainfall scenario in which either (a) <1mm of rain fell on the day of the acquisition and > 3mm fell on the previous day, or (b) <1mm of rain fell on the acquisition day and the previous day and >3mm fell on the day before that. The black line is regression R3 of table 1.

A further factor potentially affecting the difference in mean relative SSMC between low slopes near rivers and higher slopes in a 10km square might be the elevation of the square. Elevations are higher in the west of the region than the east. The influence of elevation was also examined in a regression analysis. Fig. 8 is a plot of the slope *s* of $SSMC_D$ against $SSMC_L$ versus the mean elevation of low slopes within a 10km square, for each 10km square. There appears to be no significant correlation between *s* and the mean elevation of low slopes within a 10km square, for all 10km squares (linear regression intercept = 0.0256, regression slope = 0.000055 ± 0.000241 on 45 samples, R^2 = 0.01).

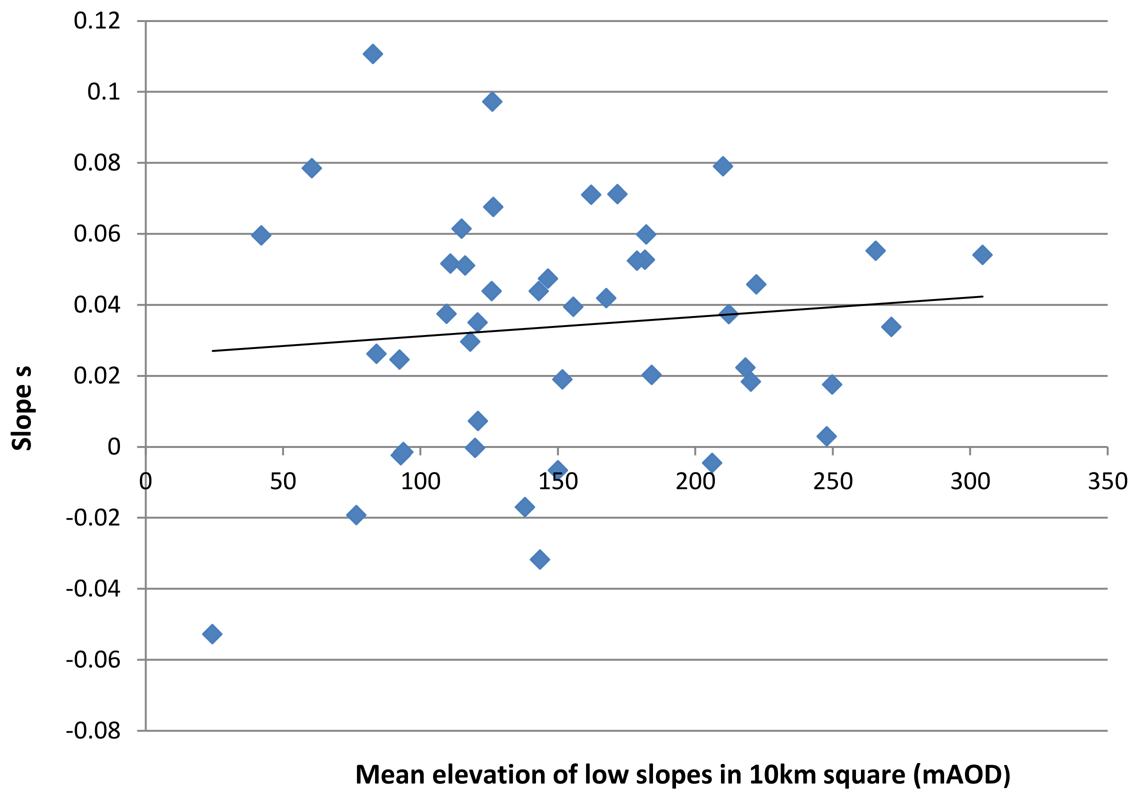

Figure 8. Slope *s* of relative SSMC difference between higher slopes and low slopes near rivers against relative SSMC of low slopes near rivers, versus mean elevation of low slopes near rivers, in each 10km square.

4.2 Changes in root zone soil moisture

While some changes in remotely sensed relative surface soil moisture content have been detected between low slopes near rivers and higher slopes in specific wetness ranges, it is still necessary to show that these are likely to result in corresponding changes in root zone soil moisture *RZSM*, because it is the latter that will be assimilated into a hydrologic model.

The exponential filter used to estimate the profile soil water index *SWI* from m_s is a weighted average of the m_s values from scenes acquired just prior to the date in question, so that changes in $m_s(t_i)$ should result in changes in *SWI*, though these may be damped by the averaging process. It could be argued that it is unnecessary to validate the remote sensing soil moisture content against ground measurements because we are simply looking for relative changes between different slopes. However, the validity of the result is reinforced if there is a reasonable correspondence between ground and remote sensing measurements of profile soil water content. A small number of ground measurements were collected at a site at Pontbren in the north-west of the region in 2006-9 (Marshal et al., 2009). A neutron probe at the site was immediately adjacent to an ASAR improved grassland pixel, though was also near trees. Ground measurements were made once every fortnight, every 10cm down to 120cm. Fig. 9 shows a comparison between the ASAR WS profile soil moisture content versus volumetric ground profile soil moisture content (0-20cm) (cm^3/cm^3) at Pontbren. The results assume a clay soil, with a wilting level of 0.15 and field capacity of 0.45 cm^3/cm^3. There does appear to be a linear relationship between remote sensing and ground measurements, though the slope of 0.72 ± 0.13 is less than one at the 5% significance level. However, it must be remembered that an areal remote sensing measurement over the ASAR pixel is being compared with a ground measurement at a point. Also, due partly to the infrequent sampling of ground measurements, there was usually a time difference of a few days (mean 3, maximum 7) between a ground measurement and the ASAR acquisition closest to it in time.

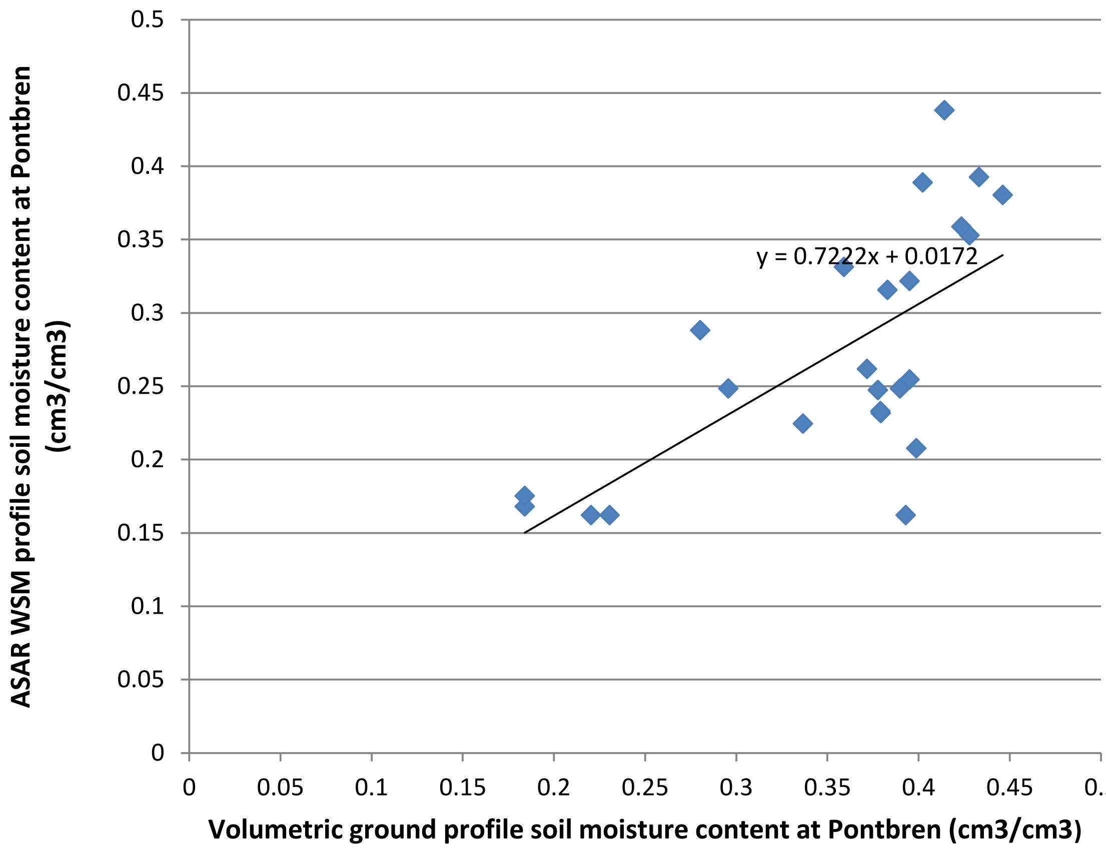

Figure 9. ASAR WS profile (0-20cm) soil moisture content versus volumetric ground profile soil moisture content (cm^3/cm^3) at Pontbren (assumes clay soil, wilting level = 0.15, field capacity = 0.45 $cm^3/cm^{3)}$.

5. Conclusion

The mean relative SSMC from improved grassland pixels on low slopes near rivers was compared to that from similar pixels on higher slopes not necessarily near rivers. The comparison was performed by averaging results from about 50 10km squares across the region, in each of which there were a substantial number of pixels in each class. It was shown that -
(a) when the mean relative SSMC on low slopes approaches 100%, there is little difference between the mean relative SSMC of the low and higher slopes,
(b) when the mean relative SSMC on low slopes is 30 - 90%, the higher slopes are slightly drier than the low slopes,
(c) when the mean relative SSMC is low, the low slopes become slightly drier than the higher slopes,
(d) if a similar comparison was made during a drying phase when rainfall occurred a day or two previously, the higher slopes became drier than the low slopes to a greater extent than in case (b) when the mean relative SSMC on low slopes was 35-70%,
(e) there appeared to be no significant correlation between the slope $d(SSMC_D)/d(SSMC_L)$ and the mean elevation of low slopes within a 10km square,
(f) based on a very limited sample of ground measurements, there appeared to be a linear relationship between remote sensing and ground profile soil moisture measurements.

This is evidence that a topographic signal can be seen in high resolution remotely sensed surface soil moisture data, which may be useful information for a hydrologic model to be able to account for spatial heterogeneity in hydrological processes. Unfortunately this signal is relatively weak.

However, a further advantage of using ASAR WS data for measuring soil moisture for assimilation into a hydrologic model is their high spatial resolution, which, when combined with a land cover map, allows soil moisture to be measured over single homogeneous pixels. This would not be the case for low resolution microwave sensors, or even for the 1km-resolution soil moisture product from Sentinel-1. While the resolution of Sentinel-1 in Interferometric Wide Swath Mode is higher than that of ASAR WS, the resolution of the latter product has been selected because the averaging of high resolution SAR measurements to a lower spatial resolution significantly reduces noise and improves radiometric resolution (Pathe et al., 2009, Doubkova et al., 2012). However, this does not rule out the possibility of deriving higher resolution soil moisture data for regions of homogeneous land cover from Sentinel-1 if required.

In this study the SSMC from improved grassland pixels on low slopes near rivers was compared to that on higher slopes not necessarily near rivers. This approach was followed because it mimics that taken by Roberts and Crane (1997), who compared ground measurements of near surface soil moisture on the floor of a valley near a river to those on the adjacent steeper valley sides. They found that areas of sloping hillside dried out faster than the valley floor, and that this acted as a control on storm-flow generation. An alternative approach worthy of future study would be to compare soil moisture values for regions having different topographic wetness indices (Beven et al., 1979).

Future work will involve the selection of a suitable distributed hydrologic model and assimilation system, the linkage of these, and the assimilation of the foregoing soil moisture data into the model to test whether model runoff prediction can be improved by assimilation. A variety of hydrologic models have been used in similar studies in the past, including TopNet (Clark et al., 2008), SAC (Crow and Ryu, 2009), MISDc (Brocca et al., 2012), GR4J (Aubert et al., 2003), CLM2.0 (Plaza et al., 2012) and SWAT (Chen et al., 2011). The assimilation system will probably be the Ensemble Kalman Filter (EnKF), previously used in a variety of hydrologic studies (e.g. Garcia-Pintado et al., 2013; Garcia-Pintado et al., submitted).

Acknowledgements

This work was funded partly under the UK Natural Environment Research Council Flooding from Intense Rainfall SINATRA project (NE/K00896X/1). Thanks are due to Moira Mason for helpful discussions.

References

Aubert, D., Loumagne, C., Oudin, L. 2003. Sequential assimilation of soil moisture and streamflow data in a conceptual rainfall–runoff model. J. Hydrology, 280, 145-161.

Balenzano, A., Mattia, F., Satalino, G,, Davidson, M.W.J. 2011. Dense temporal series of C- and L-band SAR data for soil moisture retrieval over agricultural crops. IEEE JSTARS, 4(2), 439-450.

Barrett, B.W., Dwyer, E., Whelan, P. 2009. Soil moisture retrieval from active spaceborne microwave observations: an evaluation of current techniques. Remote Sensing 1(3), 210-242.

Beven, K.J., Kirkby, M.J., Seibert, J. 1979. A physically based, variable contributing area model of basin hydrology. Hydrological Science Bulletin, 24, 43-69.

Brocca, L., Moramarco, T., Melone, F., Wagner, W., Hasenauer, S., Hahn, S. 2012a. Assimilation of surface- and root-zone ASCAT soil moisture products into rainfall-runoff modelling. IEEE. Trans. GeoScience Rem. Sens., 50(7), 2542-2555.

Brocca, L., Melone, F., Moramarco, T., Zucco, G, Wagner, W. 2012b. Soil moisture assimilation into rainfall-runoff modelling: which is the impact of the model structure on runoff predictions? Geophysical Research Abstracts, 14, EGU2012-2299.

Chen, F., Crow, W.T., Starks, P.J., Moriasi, D.N. 2011. Improving hydrologic predictions of catchment model via assimilation of surface soil moisture. Adv. Water Resources 34(4), 526-536.

Clark, M.P., Rupp, D.E., Woods, R.A., Zheng, X., Ibbitt, R.P., Slater, A.G., Schmidt, J., Uddstrom, M.J. 2008. Hydrological data assimilation with the ensemble Kalman filter: use of streamflow observations to update states in a distributed hydrological model. Adv. Water Resources, 31, 1309-1324.

Crow, W.T., Ryu, D. 2009. A new data assimilation approach for improving runoff prediction using remotely-sensed soil moisture retrievals. Hydrol. Earth. Syst. Sci., 13, 1-16.

Dostalova, A., Boubkova, M., Sabel, D., Bauer-Marschallinger, B., Wagner, W. 2014. Seven Years of Advanced Synthetic Aperture Radar (ASAR) Global Monitoring (GM) of Surface Soil Moisture over Africa. Remote Sensing, 6(8), 7683-7707.

Doubkova, M., van Dijk, A.I.J.M., Sabel, D., Wagner, W., Bloschl, G. 2012. Evaluation of the predicted error of the soil moisture retrieval from C-band SAR by comparison against modelled soil moisture estimates over Austria. Rem. Sens. Environ., 120, 188-196.

Entekhabi, D., Njoku, E.G., O'Neill, P. E., Kellogg, K. H., Crow, W. T., Edelstein, W.N., Entin, J.K., Goodman, S. D., Jackson, T. J., Johnson, J. 2010. The soil moisture active passive (SMAP) mission. Proc. IEEE 98(5), 704-716.

Hornacek, M., Wagner, W., Sabel, D., Truong, H-L., Snoeij, P., Hahmann, T., Diedrich, E., Doubkova, M. 2012. Potential for high resolution systematic global surface soil moisture retrieval via change detection using Sentinel-1. IEEE JSTARS, 5(4), 1303-1311.

Garcia-Pintado, J., Neal, J.C., Mason, D.C., Dance, S., Bates, P.D. (2013). Scheduling satellite-based SAR acquisition for sequential assimilation of water level observations into flood modelling. J. Hydrology, 495, 252-266.

Garcia-Pintado, J., Mason, D.C., Dance, S.L., Cloke, H.L., Neal, J.C., Freer, J., Bates, P.D. (submitted). Satellite-supported flood forecast in river networks: a real case study. J. Hydrology.

Greifeneder, F., Notarnicola, C., Cuozzo, G., Spindler, N., Bertoldi, G., Della Chiesa, S., Niedrist, G., Stamenkovic, J, Wagner, W. 2014. Analysis of ASAR Wide Swath Mode time series for the retrieval of soil moisture in mountainous areas. Geophysical Research Abstracts, 16, EGU2014-14383.

Gruber, A., Paloscia, S., Santi, E., Notarnicola, C., Pasolloi, L., Smolander, T., Pulliainen, J., Mittelbach, H., Dorigo, W., Wagner, W. 2014. Round Robin evaluation of soil moisture retrieval models for the MetOp-A ASCAT instrument. Geophysical Research Abstracts, 16, EGU2014-6462.

Kellndorfer, J.M., Pierce, L.E., Dobson, M.C., Ulaby, F.T. 1998. Towards consistent regional-to-global-scale vegetation characterization using orbital SAR systems. IEEE Trans. GeoScience Rem. Sens. 36(5), 1396-1411.

Kerr, Y., Waldteufel P., Wigneron J., Martinuzzi J., Font J., Berger M. 2001. Soil moisture retrieval from space: The Soil Moisture and Ocean Salinity (SMOS) mission. IEEE Trans. Geosci. Rem. Sens., 39(8), 1729–1735.

Kong, X., Dorling, S.R. 2008. Near-surface soil moisture retrieval from ASAR Wide Swath imagery using a principal component analysis. IJRS 29(10), 2925-2942.

Lacava, T., Matgen, P., Brocca, L., Bittelli, M., Pergola, N., Moramarco, T., Tramutoli, V. 2012. A first assessment of the SMOS soil moisture product with in situ and modelled data in Italy and Luxembourg. IEEE. Trans. GeoScience Rem. Sens., 50(5), 1612-1622.

Loew, A., Ludwig, R., Mauser, W. 2006. Derivation of surface soil moisture from ENVISAT ASAR WS and image mode data in agricultural areas. IEEE Trans. GeoScience Rem. Sens. 44(4), 889-899.

Marshall, M.R., Francis, O.J., Frogbrook, Z.L., Jackson, B.M., McIntyre, N., Reynolds, B., Solloway, I., Wheater, H.S. and Chell, J. (2009). The impact of upland land management on flooding: results from an improved pasture hillslope. Hydrological Processes, 23, 464-475

Morton D, Rowland C, Wood, Meek L, Marston C, Smith G, Wadsworth R, Simpson IC (2011). Final Report for LCM2007 – the new UK Land Cover Map. CS Technical Report No 11/07. Centre for Ecology & Hydrology. Natural Environment Research Council.

Parajka, J., Naeimi, V., Bloeschl, G., Wagner, W., Merz, R., Scipal, K. 2005. Assimilating scatterometer soil moisture data into conceptual hydrologic models at the regional scale. Hydrol. Earth Syst. Sci., 10, 353-368.

Parrens, M., Zakharova, E., Lafont, S., Calvet, J-C., Kerr, Y., Wagner, W., Wigneron, J-P. 2012. Comparing soil moisture retrievals from SMOS and ASCAT over France. Hydrol. Earth Syst. Sci., 16, 423-440.

Pathe, C., Wagner, W., Sabel, D., Doubkova, M., Basara, J.B. 2009. Using ENVISAT ASAR global mode data for surface soil moisture retrieval over Oklahoma, USA. IEEE Trans. GeoScience Rem. Sens. 47(2), 468-480.

Plaza, D.A., De Keyser, R., De Lannoy, G.L.M., Giustarini, L., Matgen, P, Pauwels, V.R.N. 2012. The importance of parameter resampling for soil moisture data assimilation into hydrologic models using the particle filter. Hydrol. Earth Syst. Sci. 16, 375-390.

Pratola, C., Barrett, B., Gruber, A., Kiely, G., Dwyer, E. 2014. Evaluation of a Global Soil Moisture Product from Finer Spatial Resolution SAR Data and Ground Measurements at Irish Sites. Remote Sensing, 6(9), 8190-8219.

Roberts, G., Crane, S.B. 1997. Temporal variations in near surface soil moisture at two contrasting sites in the Wye valley and their control on stormflow generation. Hydrol. Earth. Syst. Sci. 1(3), 453-461.

Smith, M.B., Koren, V., Reed, S., Zhang, Z., Moreda, F., Cui, Z., Mizukami, N., Anderson, E.A., Cosgrove, B.A. 2012. The distributed model intercomparison project – Phase 2: Movivation and design of the Oklahoma experiments. J. Hydrology, 418-9, 3-16.

Verhoest, N.E.C., Troch, P.A. 1998. Mapping basin scale variable source areas from multitemporal remotely sensed observations of soil moisture behaviour. Water Resources Res. 34(12), 3235-3244.

Vinnikov, K.Y., Robock, A., Speranskaya, N.A., Schlosser, A. 1996. Scales of temporal and spatial variability of mid-latitude soil moisture. J. Geophys. Res. 101(D3): 7163-7174.

Vorosmarty, C. J., Willmott, C. J., Choudhury, B. J., Schloss, A. L., Stearns, T. K., Robeson, S. M., Dorman, T. J. 1996. Analyzing the discharge regime of a large tropical river through remote sensing, ground-based climatic data, and modeling. Water Resources Research, 32, 3137-3150.

Wagner, W., Lemoine, G., Rott, H. 1999. A method for estimating soil moisture from ERS scatterometer and soil moisture data. Rem. Sens. Environment, 70(2), 191-207.

Wang, J.R., Shiue, J.C., Schmugge, T.J., Engman, E.T. 1989. Mapping soil moisture with L-band radiometric measurements. Rem. Sens. Environ, 27, 305-12.

Yang, G.J., Shi, Y.C., Xu, Q.Y. 2013. Estimation of Soil Moisture from Multi-Polarized Synthetic Aperture Radar Data-A Case Examination on RADARSAT-2 Product Over Wheat Growing Areas. Sensor Letters, 11 (6-7), 1081-1086.

Zribi, M., Kotti, F., Amri, R., Wagner, W., Shabou, M., Lili-Chabaane, Z, Baghdadi, N. 2014. Soil moisture mapping in a semiarid region, based on ASAR/Wide Swath satellite data. Water Resources Research, 50(2), 823-835.